

Vibrationally-resolved X-ray spectra of diatomic systems: Time-independent and time-dependent simulations

Lu Zhang¹, Minrui Wei¹, Guoyan Ge¹, and Weijie Hua^{*,1}

¹MIIT Key Laboratory of Semiconductor Microstructure and Quantum Sensing, Department of Applied Physics, School of Science, Nanjing University of Science and Technology, 210094 Nanjing, China

* E-mail: wjhua@njjust.edu.cn (W. Hua)

August 16, 2023

Abstract

We systematically investigated vibronic coupling effects in X-ray spectra of diatomic systems using time-independent (TI) and time-dependent (TD) methods. Under the TI framework, we studied 5 systems (N_2 , N_2^+ , NO^+ , CO , CO^+) in their lowest C/N/O 1s excited or ionized states, generating 10 X-ray absorption (XAS) or photoelectron (XPS) spectra using density functional theory (DFT) with two pure (BLYP, BP86) and two hybrid (B3LYP, M06-2X) functionals. Excellent agreement between theoretical and experimental spectra was found in most systems, except that in O1s XAS of CO and NO^+ , intensities of higher-energy peaks were underestimated. We established a connection between their complex vibronic structures and the significant geometrical changes induced by the O1s hole. Functional dependence in diatomic systems is generally more pronounced than in polyatomic ones. In all examined cases, pure functionals exhibit better or similar spectral accuracy to hybrid functionals, attributed to superior prediction accuracy in bond lengths and vibrational frequencies. With the TD wavepacket method, we simulated vibrationally-resolved XAS of CO^+ , NO^+ , and CO using potential energy curves (PECs) generated at both DFT and multiconfigurational levels. Both TD and TI generate similar C/O 1s XAS spectra of CO^+ . For O1s XAS of NO^+ and CO, TD calculations significantly improved the corresponding TI results, demonstrating sensitivity to the anharmonic effect and the PEC quality. TI and TD approaches are complementary, with practical applications depending on the ease and accuracy of excited-state geometry optimization or PEC scanning, and the significance of anharmonicity. DFT with pure functionals is recommended for diatomic calculations due to its easy execution and reliable accuracy. TI is optimal for

most scenarios, but TD is needed for problems with strong anharmonic effects.

Contents

1	Introduction	2
2	Methodology	5
2.1	Notations	5
2.2	Time-independent method	5
2.3	Time-dependent wavepacket method	6
3	Computational details	7
3.1	Time-independent calculations	7
3.1.1	Electronic structures	7
3.1.2	Spectral calculations	7
3.2	Time-dependent calculations	8
3.2.1	Potential energy curves by DFT	8
3.2.2	Potential energy curves of CO ⁺ by RASSCF	8
3.2.3	Wavepacket simulations	8
4	Results and Discussion	9
4.1	Time-independent results	9
4.1.1	Bond lengths and core-hole induced changes	9
4.1.2	Vibrational frequencies and core-hole induced changes	10
4.1.3	XAS/XPS of diatomic systems: A general overview	11
4.1.4	XAS of N ₂ and N ₂ ⁺	11
4.1.5	XAS of NO ⁺	12
4.1.6	XAS of CO and CO ⁺	13
4.1.7	XPS of CO	13
4.2	Time-dependent results	13
4.2.1	Potential energy curves of CO ⁺	13
4.2.2	Potential energy curves of NO ⁺ and CO	14
4.2.3	C1s and O1s XAS of CO ⁺	15
4.2.4	O1s XAS of NO ⁺ and CO	15
5	Summary and Conclusions	16

1 Introduction

Spectroscopy serves as a crucial link between experimental observations and theoretical understanding in physics, with precision being the key factor. One notable example in the history of physics is the hydrogen spectrum, where increasing measurement precision has reciprocally fostered the development of quantum theory. High-resolution spectroscopy acts as a litmus test for assessing

the precision of the theoretical methods employed. Particularly, in the context of high-resolution vibrationally-resolved X-ray spectroscopy,[1, 2, 3, 4, 5, 6, 7, 8, 9, 10, 11, 12, 13, 14, 15, 16] comparison to experimental data affords an evaluation of the quality of potential energy surfaces (PESs) for both the core-electron excited (or ionized) and the ground electronic states. It also provides insights into the accuracy of the electronic structure methods used, especially for states with a core hole.

In physics and chemistry, many problems can be solved either in the frequency domain or the time domain. While these two approaches are theoretically equivalent, one may be numerically superior to the other in certain cases, and some approximations or effects are more easily considered in one domain than the other. Regarding vibronic coupling, two complementary solutions exist: the time-independent (TI) framework and the time-dependent (TD) framework. The TI method, usually based on the harmonic oscillator approximation, is mathematically represented by an analytical sum-over-states expression.[17] When the Duschinsky rotation (DR) effect[18] is taken into account, the calculation involves optimizing the structure of the final state and performing vibrational frequency calculations, which can be challenging for certain systems.[19, 20] However, the spectral interpretations obtained through the TI approach are direct and straightforward, and they provide information about the structural changes induced by the core hole.[19, 20] On the other hand, the TD wavepacket method relies on the Fourier transform of the auto-correlation function.[21, 22] This method allows for the inclusion of anharmonic effects that can be included from the input PESs.

Accurate simulation of high-resolution vibrationally-resolved X-ray spectra depends both on the method to consider the vibronic coupling effect and the underlying electronic structure method used. In terms of electronic structure, density functional theory (DFT) has emerged as a predominant method that offers profound insights into a wide range of molecules and materials. DFT has demonstrated the capability to accurately predict X-ray spectra.[23] When combined with the Duschinsky rotation[18] method, it has shown good agreement with experiments for vibrationally-resolved X-ray photoelectron (XPS)[24, 19, 25] and absorption (XAS)[26] spectra of a comprehensive spectrum of molecules, such as benzene,[24] furan,[24] pyridine,[24] azines,[19] indoles,[20] polycyclic aromatic hydrocarbons (PAHs),[25] and ions like N_2H^+ .[26] In these calculations, either full core-hole (FCH) or excited core-hole (XCH)[27] approximation was leveraged to describe the core ionized (in the case of XAS) or excited (in the case of XPS) states, while conventional DFT was employed to model the ground state (GS). (In the subsequent context, the term “excited state” is used without distinction to refer to either a core excited or ionized state.) It is worth noting of other DFT applications[8, 28, 24] also with the half core hole (HCH)[29] or the equivalent core hole (ECH, i.e., $Z+1$)[30] approximations. Buoyed by the promising outcomes from DFT computations, we are currently engaged in formulating a theoretical library for vibrationally-resolved XPS/XAS spectra of common molecules and ions, with initial findings already disseminated.[24, 19, 20, 25] Most investigated systems were polyatomic, i.e.,

composed of three or more atoms.

Diatomic systems, with a single vibrational mode, offer a more “transparent” view of vibronic coupling effects and are highly sensitive to the utilized vibronic coupling and the electronic structure methods. Extensive investigations have been conducted on diatomic molecules such as N_2 , [31] CO , [32] NO , [32] and ions like NH^+ , [33] N_2^+ , [34] CO^+ , [22] NO^+ , [35] and C_2^- [16] through both XPS and XAS experiments, [31, 32, 2, 33, 34, 22, 35, 16] as well as theoretical simulations at various levels. [1, 31, 32, 33, 34, 22, 35, 16] Generally, good agreement between experimental and theoretical results has been observed. Alongside technological advancements in X-ray synchrotron beams for experimental development [11], theoretical methods for X-ray spectra have also seen significant improvements in recent years, [1] enabling high-quality theoretical predictions of vibrationally resolved X-ray spectra. Neutral diatomic molecules have been a frequent focus in many X-ray spectral studies due to their ability to reach higher target densities compared to charged particles. [16] Recent innovations in ion beam and ion trap techniques have facilitated precise inner-shell investigations involving positively charged diatomic molecular ions. [35, 33]

Previously various post-Hartree-Fock methods were used in almost all diatomic calculations. Couto et al. [22] presented and analyzed high-resolution XAS spectra of CO^+ by employing wavepacket dynamics calculations based on potential energy curves (PECs) computed with the restricted active space second-order perturbation (RASPT2) method. Lindblad et al. [35] interpreted the experimental XAS spectra of N_2^+ [34] and NO^+ using the restricted active space multiconfigurational theory self-consistent field (RASSCF) and RASPT2 methods. Carniato et al. [33] simulated the PECs of low-lying N1s excited states of NH^+ by using the configuration interaction singles and doubles (CISD) method and the valence-state PECs by multiconfigurational self-consistent field (MCSCF). Rocha [36] simulated PEC of CO in the lowest C1s excited state by the restricted active space SCF (RASSCF) method, termed also as the inner-shell complete active space SCF (IS-CASSCF) method. Martins et al. [37] computed PECs of low-lying F1s core excited states of HF and HF^+ by using the full configuration-interaction method to help understand the photodissociation dynamics. Such studies have been instrumental in enriching our understanding of core-hole state electronic structure, X-ray physics, vibronic coupling, and bond dissociation dynamics. However, such studies typically focus on one or only a few systems, and computational studies by different groups often employ different theoretical levels. The lack of simulations for multiple systems on the same footing hinders fair comparisons and the derivation of general rules regarding vibronic coupling properties.

The goal of the present study is to utilize both the TI and TD methods in order to get a complete picture of vibrationally-resolved X-ray spectral simulations for diatomic systems. In the TI framework, we aim to benchmark DFT in simulating vibrationally-resolved XPS/XAS spectra of diatomic systems. Despite potential limitations at larger bond distances where multiconfigurational effects are crucial, DFT has demonstrated the ability to generate accurate PECs near the Franck-Condon region. The FCH approximation will be utilized for

the lowest 1s ionized state, while the XCH approximation will be employed for the lowest 1s excited state. The XAS spectra of common molecules and ions (N_2 , N_2^+ , NO^+ , CO , and CO^+), as well as the XPS spectra of CO , covering the C/N/O K-edges, will be considered.

This study will also present time-dependent results for selected systems (CO^+ , CO , NO^+). In addition to the four DFT methods, we will also compute the spectra with multiconfigurational methods for comparisons, with the input potential energy curves (PECs) generated by us or obtained from previous publications. This work is also motivated by a previous study[26] (by one of the coauthors, WH) on a triatomic system, NH_2^+ , where DFT well predicted the double-well potentials of the lowest N1s excited states of both nitrogens (along one of the bending vibrational modes) and generated good XAS spectral agreement with the experiment. Through the current comprehensive investigation, valuable insights are expected to be provided for accurate and efficient simulations by combining different electronic structure and vibronic coupling methods, thereby advancing both the theoretical framework and practical applications in high-resolution X-ray spectroscopy.

2 Methodology

2.1 Notations

We use bolded symbols in lower and upper cases for vectors and matrices, respectively, while symbols in normal fonts indicate scalars. The initial (ground) electronic state is denoted by g , and the final (core-excited or core-ionized) electronic state by e . We differentiate any physical quantity in state g or e using a respective symbol with or without a prime. As such, equilibrium geometries (expressed as Cartesian coordinates in column vectors) of the initial and final states are denoted by \mathbf{x}' and \mathbf{x} ; normal coordinates (also in column vectors) for both states are represented by \mathbf{q}' and \mathbf{q} ; respective normal mode matrices are signified by \mathbf{L}' and \mathbf{L} ; vibrational frequencies are designated by ω' and ω ; and bond lengths are represented by R' and R .

2.2 Time-independent method

The time-independent method was considered based on the harmonic oscillator approximation. Vibrational frequency calculations were first performed at the optimized geometries of both the initial and the final electronic states. The Duschinsky rotation (DR) method[18] was then used to connect both normal coordinates:

$$\mathbf{q}' = \mathbf{J}\mathbf{q} + \mathbf{k}. \quad (1)$$

Here \mathbf{k} indicates the displacement vector between the PESs of both electronic states along the normal coordinate. \mathbf{J} is the Duschinsky rotation matrix, which is 1 for a diatomic system. \mathbf{k} depends on the initial-state normal coordinate

matrix \mathbf{L}' , the diagonal matrix of atomic masses \mathbf{M} , and the change between the equilibrium geometries of both states $\Delta\mathbf{x}$ ($\Delta\mathbf{x} \equiv \mathbf{x} - \mathbf{x}'$):

$$\mathbf{k} = (\mathbf{L}')^T \mathbf{M}^{1/2} \Delta\mathbf{x}. \quad (2)$$

The vibrational profile can then be calculated with \mathbf{k} and the vibrational frequencies (ω' and ω).[38, 39, 40]

The 0-0 vibrational transition energy in XAS and XPS spectra are respectively calculated by using the Δ Kohn-Sham (Δ KS) scheme,[41, 42]

$$\begin{aligned} E_{00}^{\text{XAS}} &= E_{\text{XCH}}|_{\text{min XCH}} - E_{\text{GS}}|_{\text{min GS}} + \delta_{\text{rel}}, \\ E_{00}^{\text{XPS}} &= E_{\text{FCH}}|_{\text{min FCH}} - E_{\text{GS}}|_{\text{min GS}} + \delta_{\text{rel}}, \end{aligned} \quad (3)$$

which considers both electronic and geometrical relaxations. Here E_{GS} , E_{FCH} , and E_{XCH} stand for total energies of the ground electronic state, the FCH state with one 1s electron removed, and the XCH state with one 1s electron excited to the lowest unoccupied molecular orbital (LUMO), respectively; **min GS**, **min FCH**, or **min XCH** denotes the optimized structure of each state. δ_{rel} is a small uniform shift considering the differential relativistic effect, which is related to the removal of an electron from the core orbital. The values used for the C, N, and O 1s core holes are $\delta_{\text{rel}} = 0.2, 0.3,$ and 0.4 eV, respectively.[42]

2.3 Time-dependent wavepacket method

We take the vibrationally-resolved XAS spectroscopy as an example and present the essentials of the time-dependent wavepacket method. ω_g and ω_e are used to denote the total energies of the ground and core-excited states, respectively. By assuming that the photon absorption process is sudden, the initial ($t = 0$) wavepacket of the core-excited state is just the ground state vibrational wavefunction of the ground electronic state, i.e., $|\psi_e(t = 0)\rangle = |\psi_{g0}\rangle$. The time evolution of the wavepacket can be considered as free propagation of $|\psi_{g0}\rangle$, i.e.,

$$|\psi_e(t)\rangle = e^{-i\hat{H}_e t} |\psi_{g0}\rangle. \quad (5)$$

Here \hat{H}_e is the nuclear Hamiltonian of the core-excited state. By computing the overlap integral with the initial state (i.e., the auto-correlation function),

$$\sigma_e(t) = \langle \psi_{g0} | \psi_e(t) \rangle, \quad (6)$$

the X-ray absorption cross section at incident photon energy ω can be calculated via a half Fourier transform of σ_e : [21]

$$\sigma_{\text{XAS}}(\omega) = -\frac{V_{ge}^2}{\pi} \text{Re} \int_0^\infty dt e^{i(\omega - \omega_{eg} + E_{g0})t - \Gamma t} \sigma_e(t). \quad (7)$$

Here V_{ge} is the transition dipole moment between electronic states g and e , $\omega_{eg} \equiv \omega_e - \omega_g$ stands for the electronic transition energy, E_{g0} represents the energy of the ground vibrational state of the ground electronic state, Γ is the hwhm

core hole lifetime broadening. In practice, since only one electronic state was considered in this work, V_{ge}^2 is just a constant term and was omitted. The same working formula to Eq. 7 applies to the vibrationally-resolved XPS spectrum except that the index e means the core-ionized state.

3 Computational details

3.1 Time-independent calculations

3.1.1 Electronic structures

All electronic structure calculations were carried out at the DFT level by using the GAMESS-US package,[43] enforcing a C_{4v} point group symmetry. Four different functionals were chosen: BLYP,[45, 46] BP86,[45, 47] B3LYP,[48, 46] and M06-2X.[49] A double basis set technique was used.[24] The aug-cc-pVTZ basis set[50] was used in the geometrical optimization of the ground state. Concerning the excited state, the IGLO-III basis set[52] was set for the excited atom. The basis set for the other atom was chosen as follows: in a homonuclear molecule or ion (N_2 , N_2^+), model core potential (MCP) together with corresponding MCP/TZP basis set[53] was employed; while in a heteronuclear system (CO , CO^+ , NO^+), the aug-cc-pVTZ basis was set. Unrestricted DFT (UDFT) was employed for all excited-state calculations except for 1s ionized states of CO , where UDFT encountered SCF convergence errors, and restricted open-shell DFT (RO-DFT) was used instead. Vibrational frequency calculations were then performed at the optimized structures (all Cartesian coordinates provided in the Supplementary Material[56]).

3.1.2 Spectral calculations

Then, a modified DynaVib package [24] was employed to compute the Franck-Condon factors (FCFs) based on the obtained energies, geometries, and vibrational frequencies. The vibrationally-resolved XAS and XPS spectra were obtained by convoluting the stick FCFs with a Lorentzian function. A hwhm value, $\gamma=0.05$ eV, was chosen to achieve better agreement with experimental observations. Here γ is to phenomenologically include many effects for broadening (such as the lifetime, instrumental, and Doppler broadening, and environmental effects) and similar values have been utilized in previous studies for other systems.[24, 19, 20, 25] In principle, one may always use the Voigt convolution (see, e.g., Ref. [26]) to tune a better agreement with the experiment, with the Lorentzian/Gaussian hwhm components read either from a library,[57] or directly from the experiment.[26] Nevertheless, in this work, the hwhm parameter is not a pivotal factor. For simplicity and consistency, a constant hwhm value was utilized in all calculations, which does not impact the validity of our discussions.

3.2 Time-dependent calculations

3.2.1 Potential energy curves by DFT

The potential energy curves for all three systems (CO^+ , CO , NO^+) were generated using density functional theory (DFT) implemented in the GAMESS-US package.[43]. For CO^+ , both the ground state and the lowest C1s and O1s excited states were considered, while for NO^+ or CO , the ground the lowest O1s excited states were studied. Four different functionals were employed: BLYP,[45, 46] BP86,[45, 47] B3LYP,[48, 46] and M06-2X.[49] The IGLO-III basis set[52] was set for the excited atom and the aug-cc-pVTZ basis set[50] for the other atom. The PEC scan ranges from 0.800 to around 1.600 Å with an incremental of 0.020 Å. In generating the final-state PEC, the converged molecular orbital (MO) from the previous geometry served as the initial guess for the consequent step, ensuring a smooth PEC. In practice, more points were generated at larger distances beyond a certain threshold, determined by observing nonphysical discontinuities indicative of DFT’s limitations at large distances. The resulting PECs were fitted with Morse potentials and extrapolated up to 4.000 Å.

3.2.2 Potential energy curves of CO^+ by RASSCF

For a selected system CO^+ , PECs were generated at the RASSCF level by using the Molpro package.[58] These include the ground, the lowest C1s and O1s excited states. The C_{2v} point group symmetry was enforced at each point. The aug-cc-pVTZ basis set was employed. In the electronic structure calculations for each snapshot, the state-averaged CASSCF method was employed to calculate the ground-state PEC. The active space consisted of 9 electrons in 7 orbitals, including 2 σ , 1 σ^* , 2 π , and 2 π^* orbitals. Three low-lying valence-excited states each were considered for state averaging in the a_1 , b_1 , and b_2 irreducible representations. Then, the C/O 1s core-excited state PECs were simulated using the RASSCF(11, 1/7/0) method, where the numbers in parentheses represent the total number of active electrons and the size of the RAS1/RAS2/RAS3 spaces. In order to obtain an energy range suitable for spectral analysis, 15 states were averaged for each symmetry (a_1 , b_1 , and b_2) at both the C and O K-edges. The core orbital was always frozen in the RAS1 space, with an electron occupation number fixed at 1. These procedures have been previously adopted and validated for generating accurate X-ray absorption spectra.[59, 60, 61].

3.2.3 Wavepacket simulations

Taking the PECs generated above as inputs, vibrationally-resolved XAS spectra of the three diatomic systems (CO^+ , CO , NO^+) were computed by wavepacket simulations using our in-house XSpecTime program.[62] Besides, we also recaptured PEC data from the literature, including PECs of CO^+ generated at the RASPT2 level by Couto et al.[22] (ground and the lowest C1s and O1s excited

states), and PECs of CO generated at the third-order multireference perturbation theory (MRPT3) level by Huang et al.[15] (ground and the lowest O1s excited states). Our tests have shown that the spectra calculated by our code closely match those reported previously,[22, 15] validating our wavepacket code and providing more extensive comparisons.

The program first reads two sets of PECs, corresponding to the initial and final electronic states, generated by the same electronic structure method (DFT, RASSCF, RAPT2, or MRPT3). Then the spectrum was calculated at 201 discrete points ranging from 0.800 to 4.000 Å. The wavepacket propagation was performed with a time step of 1.0 atomic units (a.u.), a total simulation time of 6×10^6 a.u., and a core hole lifetime of 0.05 eV. It is worth noting that the chosen constant lifetime is the same as that used in the TI study, allowing for a better comparison between the TD and TI simulations. Furthermore, validations have been conducted using shorter time steps and longer simulation times, and the resulting spectra remain unchanged.

4 Results and Discussion

4.1 Time-independent results

4.1.1 Bond lengths and core-hole induced changes

Table 1 displays the theoretical bond lengths for each system in the optimized ground state (R') and excited state (R), as well as their differences denoted by $\Delta R \equiv R - R'$. A comparison with gas phase experiments is also provided to illustrate the performance of four different functionals. Figure 1 offers a more visual representation of the comparisons. The ground-state experimental bond lengths of these systems (in the gas phase) fall within a narrow range of $R' = 1.063\text{--}1.128$ Å, spanning a difference of 0.065 Å. In the excited states, the bond lengths cover a much wider range of 0.228 Å ($R = 1.063\text{--}1.291$ Å). The 1s core excitation/ionization can lead to both increases (by 0.025–0.163 Å) or decreases (by 0.037–0.065 Å) in bond lengths, depending on the system and the excited atom. This corresponds to positive or negative values of ΔR [see Fig. 1(b)].

Our theoretical results obtained from all functionals generally exhibit good agreement with the experiments [Table 1; Fig. 1(a)]. The mean absolute deviations (MADs) for R (R') predicted by BLYP, BP86, B3LYP, and M06-2X functionals are 0.008, 0.006, 0.008, and 0.014 Å (0.008, 0.008, 0.005, and 0.010 Å), respectively. The maximum absolute deviations (MAXs) are 0.017, 0.017, 0.027, and 0.037 Å (0.010, 0.010, 0.011, and 0.017 Å). The corresponding relative errors for R (R') are 0.2%–1.6%, 0.0%–1.6%, 0.1%–2.3%, and 0.2%–3.4% (0.0%–0.9%, 0.1%–0.9%, 0.2%–1.0%, and 0.5%–1.5%). Regarding ΔR , the deviations from experiments are 0.001–0.008, 0.000–0.007, 0.001–0.020, and 0.001–0.022 Å, respectively. These deviations from experiments are almost imperceptible for R or R' [Fig. 1(a)] and small for ΔR [Fig. 1(b)].

The results show that the pure functionals (BLYP and BP86) generally provide better agreement with the experiments than the two hybrid functionals (B3LYP and M06-2X). Specifically, with the two pure functionals, the best agreement with the experiment[34] is observed in N_2^+ , with absolute deviations of only 0.000-0.002 Å for R and R' . This is followed by N_2 , which shows absolute deviations of merely 0.000-0.005 Å in comparison to the experiment.[63] The corresponding deviations in ΔR for N_2^+ and N_2 are found to be 0.002–0.002 and 0.003–0.005 Å, respectively. On the other hand, B3LYP and M06-2X predict the least agreement in terms of ΔR for N_2^+ and N_2 among all examples illustrated in Fig. 1(b). Specifically, the deviations of ΔR by B3LYP are 0.014 and 0.020 Å for both systems, while those by M06-2X are 0.021 and 0.022 Å. These findings highlight the superior performance of the pure functionals BLYP and BP86 in accurately predicting the bond lengths.

4.1.2 Vibrational frequencies and core-hole induced changes

Table 2 presents the vibrational frequencies in the initial (ω') and final (ω) states, along with comparisons to experimental values. The experimental vibrational frequencies span a range of 2169.8–2376.7 cm^{-1} (with a difference of 206.9 cm^{-1}) in the ground state geometry, and a much wider range of 1338.9–2507.6 cm^{-1} (with a difference of 1168.7 cm^{-1}) in the excited state. The values correspond to typical frequencies for stretching vibrational modes. Similarly to the bond lengths, the influence of the core hole on vibrational frequencies does not follow a definite trend, as both frequency increases and decreases are observed.

The deviations between our DFT calculations to experiments appear to be larger for frequencies compared to bond lengths. This is because vibrational frequency corresponds to the second-order energy derivatives of the Cartesian coordinates. The mean absolute deviations for BLYP, BP86, B3LYP, and M06-2X are 38.5, 33.8, 111.7, and 200.7 cm^{-1} for ω (and 44.2, 34.5, 73.3, and 156.0 cm^{-1} for ω'). The maximum deviations are 74.1, 73.0, 315.0, and 475.4 cm^{-1} for ω (and 55.3, 48.8, 122.8, and 210.9 for ω'). The relative deviations for ω (ω') are 0.9%–5.5%, 0.1%–3.7%, 0.4%–13.0%, and 2.3%–20.0% (1.0%–2.6%, 0.6%–2.3%, 1.9%–5.6%, and 4.8%–9.1%). Table 2 also shows the vibrational frequency change between the initial and final states, denoted by $\Delta\omega \equiv \omega - \omega'$. Correspondingly, the deviations in $\Delta\omega$ are found to be in the range of 3.5–82.0, 2.0–96.2, 11.4–192.2, and 12.5–275.7 cm^{-1} .

The deviations for ω' or ω are small for the pure functionals and acceptable for the hybrid functionals, as shown in Fig. 1(c). In terms of $\Delta\omega$, the deviations by BLYP or BP86 are small, while the results by B3LYP or M06-2X are acceptable for most examples, as displayed in Fig. 1(d). The largest deviation occurs in N_2^+ , with a value of 192.2 cm^{-1} by B3LYP and 275.7 cm^{-1} by M06-2X, respectively.

The analysis of vibrational frequencies supports the same conclusion as the bond lengths, namely that the pure functionals yield better results compared to the hybrid functionals. Our DFT calculations demonstrate reasonable accuracy in predicting vibrational frequencies, considering the absolute values of experi-

mental frequencies are some 2100-2400 cm^{-1} in the ground state and 1300-2500 cm^{-1} in the excited state. Moreover, our calculations show balanced accuracy in both the ground and excited states, as indicated by the similar MAD values for the same functional. Similar levels of accuracy have been reported in other studies. For instance, Moitra et al.[64] achieved an overestimation of 90 cm^{-1} (2233 cm^{-1} predicted *versus* 2143 cm^{-1} experimental) and 102 cm^{-1} (2432 cm^{-1} predicted *versus* 2330 cm^{-1} experimental) for CO and N₂, respectively, in the ground state by using the MP2 method.

4.1.3 XAS/XPS of diatomic systems: A general overview

Figures 2-5 illustrate the simulated vibrationally-resolved XAS spectra of N₂, N₂⁺, NO⁺, CO, and CO⁺ computed using DFT with four different functionals, which will be discussed in detail in subsequent sections. In most case studies, theoretical results demonstrate good agreement with experimental observations. Noticeable differences by different functionals can often be observed, although the level of sensitivity may vary depending on the specific system and spectroscopy being studied.

It is generally observed that functional dependence is more pronounced in diatomic molecules compared to polyatomic ones. For instance, weak functional dependence was observed in the vibrationally-resolved N1s XPS spectrum of pyrimidine (C₄H₄N₂).[19] The functional sensitivity appears to be diminished in polyatomic systems due to the presence of multiple vibrational modes. That is, the combined effects of various vibrational modes tend to wash out the functional dependence.

4.1.4 XAS of N₂ and N₂⁺

Figure 2 presents our computed N1s XAS spectra of N₂ and N₂⁺ compared with the experiments.[6, 65, 34] In Fig. 2(a), the experimental spectrum exhibits five distinct vibronic features, with the 0-0 and 0-1 peaks having nearly equal intensities. Our BLYP and BP86 calculations accurately predict the peak separations (corresponding to the vibrational frequencies) and relative peak intensities. In a diatomic system, the peak separation is equivalent to the vibrational frequency, and the agreement in separation here is consistent with the discussion in Section 4.1.2 (also refer to Table 2). BLYP yields almost identical intensities for the 0-0 and 0-1 peaks, showing the best agreement with the experiment. BP86 shows a slightly weaker 0-1 peak than the 0-0 peak. On the other hand, B3LYP and M06-2X predicted relatively large peak separations and the 0-1 peak intensity is approximately two-thirds of the 0-0 peak. Overall, our results suggest that pure functionals perform better than hybrid functionals in this case.

In Fig. 2(b), the 0-0 experiment peak of N₂⁺ (394.29 eV) experiences a red-shift of 7.20 eV compared to N₂ (401.49 eV), which is consistent with valence shell ionization. Additionally, three vibronic features are evident in the experimental spectrum, with the 0-1 peak having approximately half the intensity of the 0-0 peak. Similarly, BLYP and BP86 predict peak separations in good

agreement with the experiment and reproduce the relative peak intensities with a slight underestimation of the 0-1 peak intensities. On the other hand, B3LYP and M06-2X slightly overestimate the peak separations and the 0-1 peak intensity compared to the 0-0 peak. They exhibit a slower decay in intensity with respect to the increasing vibrational quantum number n , compared to the experimental trend.

4.1.5 XAS of NO⁺

Figure 3(a-b) displays the XAS results of NO⁺ at both the N1s and O1s edges. In the N1s edge (panel a), all four functionals show good agreement with the experimental spectrum,[35] which exhibits five distinct vibronic features with approximately equal intensities for the 0-0 and 0-1 peaks. The pure functionals accurately predict the peak separations, although they slightly underestimate the intensity of the 0-1 peak and exhibit a faster decay with increasing vibrational quantum number n . On the other hand, the hybrid functionals (B3LYP and M06-2X) slightly overestimate the peak separations but match the experiment well in terms of peak intensities, with the 0-0 and 0-1 peaks having similar intensities.

In the O1s edge (panel b), the experimental spectrum[35] displays more complex structures with ten relatively weak vibronic features. To some extent, it seems challenging to accurately identify the 0-0 peak. All four functionals yield similar theoretical spectra that show only acceptable agreement with the experiment. While the general shapes of the peak profiles are consistent, the theories underestimate the peaks in the higher-energy region (i.e., those with larger vibrational quantum numbers n).

The discrepancy between the theoretical and experimental XAS spectra in the O1s edge of NO⁺ can be attributed to the harmonic oscillator approximation used. In this case, a better agreement with the experiment was achieved by considering anharmonic effects through the use of RASPT2 potential energy curves.[26] The underlying electronic structure reason lies in the fact that O1s core excitation in NO⁺ induces a large change in the PEC, including shifts in equilibrium position and alterations in curvature. As mentioned above, the O1s core excitation in NO⁺ led to a bond length increase of +0.140 Å (from 1.063 to 1.203 Å) and a decrease in vibrational frequency of -841.8 cm⁻¹ (from 2376.7 to 1534.9 cm⁻¹). Among all the examples studied, they represent the second largest bond length change (Table 1) and the largest vibrational frequency change (Table 2), respectively. Additionally, we think the anharmonic effect can be decomposed into two parts: one originating from the vibronic coupling method and the other from the electronic structure method. It would be interesting to separate these two parts through wavepacket simulations based on PECs generated by DFT. This will be covered in the TD study in Section 4.2.4.

4.1.6 XAS of CO and CO⁺

Figure 4(a-b) shows the XAS spectra of CO in both the C1s and O1s edges. CO and NO⁺ are isoelectronic species. The results of CO show very similar performance to NO⁺. In the C1s edge (panel a), the experimental spectrum exhibited only two simple features, while the O1s edge (panel b) displayed approximately 12 weak features within a broad peak. All functionals produced spectra with weak functional dependence. They all predict good agreement to the experiment in the C1s edge and acceptable agreement in the O1s edge. In the O1s edge, all theories underestimated the intensities for high-energy features, similar to the case of NO⁺ in the O1s edge. The underlying structural reason is also the significant changes in the PEC as induced by O1s core excitation. Specifically, the bond length increased by +0.163 Å (from 1.128 to 1.291 Å) and the vibrational frequency decreased by -830.9 cm⁻¹ (from 2169.8 to 1338.9 cm⁻¹). Among all examples studied, they refer respectively to the largest change in bond length (Table 1) and the second-largest change in vibrational frequency (Table 2).

The case of CO⁺ is much simpler. Figure 5 displays the XAS spectra of CO⁺ in both the C1s and O1s edges. The valence-shell ionization from CO to CO⁺ resulted in a red shift of the experimental 0-0 peak in both edges: -5.25 eV (from 287.29 to 282.04 eV) in the C1s edge and -5.20 eV (from 533.62 to 528.42 eV) in the O1s edge. In both edges, all four functionals achieved good agreement with the experiment[22] in terms of energies and profiles, exhibiting only weak functional dependence.

4.1.7 XPS of CO

All examples above are on XAS spectra. Shifting our focus to XPS spectra, Fig. 6 presents the simulated vibrationally-resolved XPS spectra of CO at the C and O 1s edges. In comparison to the XAS experiments, the 0-0 peak in both edges exhibits blue shifts: +8.84 eV (from 287.29 to 296.13 eV) and +9.00 eV (from 533.62 to 542.62 eV). The experimental XPS spectra[2] show simple vibronic features at both edges, and all four functionals accurately reproduced the experimental spectra. However, it should be noted that the hybrid functional M06-2X slightly overestimated the intensity of the 0-1 peak in the C1s edge [Fig. 6(a)].

By comparing the XAS [Fig. 4(b)] and XPS [Fig. 6(b)] spectra of CO at the O1s edge, one can find the different responses of the final-state PEC induced by O1s excitation and ionization. This may be related to the odd or even number of electrons.

4.2 Time-dependent results

4.2.1 Potential energy curves of CO⁺

Figure 7 displays the ground and 1s core-excited state PECs of CO⁺ predicted by various methods. The PECs are fitted to the Morse potential, and the resulting parameters are listed in Table 3. In the ground electronic state (bottom), the

four DFT methods and the two multiconfigurational methods exhibit similar profiles. The equilibrium positions (R_e) range from 2.066 to 2.121 bohr, with relative errors varying from 0.55% (BP86) to 1.99% (M06-2X) when compared to the experiment bond length of 2.108 bohr (1.115 Å).[63] The deviations in equilibrium positions are also similar to bond lengths obtained from geometry optimizations in the TI framework, which range from 0.45% (B3LYP) to 1.17% (M06-2X)

Larger discrepancies are observed in PECs of the lowest C1s and O1s excited states. In the C1s state (Fig. 7, middle), R_e ranges from 1.990 to 2.039 bohr, while in the O1s state (top), R_e ranges from 2.134 to 2.222 bohr. The corresponding relative errors vary from 0.20% (RASPT2) to 1.95% (RASSCF) and from 0.04% (B3LYP) to 2.87% (RASSCF), respectively, when compared to experimental values (C1s, 2.029 bohr or 1.078 Å; O1s, 2.197 bohr or 1.162 Å).[22] Note that bond lengths obtained from geometry optimizations have relative errors in a similar degree: 0.19% (BLYP and BP86)–1.76% (M06-2X) and 0.09% (B3LYP)–1.20% (BLYP) in the lowest C1s and O1s excited states, respectively.

In the ground state, the fitted dissociation energy or well depth (D_e) falls within the range of 0.32–0.37 a.u., with the RASSCF method yielding the smallest value and M06-2X producing the largest value. In the two excited states, D_e ranges 0.31–0.46 a.u. and 0.24–0.35 a.u., respectively.

4.2.2 Potential energy curves of NO⁺ and CO

The PECs of NO⁺ and CO predicted by different methods are shown in Fig. 8(a) and 8(b), respectively. In the ground state of NO⁺ [Fig. 8(a), bottom], R_e ranges from 2.000 to 2.039 bohr, while in the O1s excited state (top), R_e ranges from 2.218 to 2.277 bohr. The corresponding relative errors vary from 0.21% (B3LYP) to 1.48% (BLYP) and from 0.13% (BLYP) to 2.48% (M06-2X), respectively, when compared to experimental values of 2.009 and 2.274 bohr (1.063 and 1.203 Å)[63].

In the ground state of CO [Fig. 8(b), bottom], R_e ranges from 2.129 to 2.157 bohr, while in the O1s excited state (top), R_e ranges from 2.385 to 2.448 bohr. The corresponding relative errors vary from 0.12% (MRPT3) to 1.15% (BP86) and from 0.10% (BLYP) to 2.25% (M06-2X), respectively, when compared to experimental values of 2.132 and 2.440 bohr (1.128 and 1.291 Å).[63]

For both systems, the relative deviations in equilibrium positions from Morse fitting are in a similar range as those of the optimized bond lengths in the TI approach. Concerning the dissociation energy, for NO⁺, the fitted D_e falls within the range of 0.47–0.67 and 0.16–0.21 a.u. in both the initial and final states, with the smallest by BLYP and the largest by M06-2X, respectively. For CO, the fitted D_e values in both electronic states are in the range of 0.41 (BLYP) – 0.54 (M06-2X) a.u. and 0.14 (B3LYP) – 0.19 (M06-2X) a.u., respectively.

4.2.3 C1s and O1s XAS of CO⁺

Figure 9(a) depicts the C1s XAS spectra of CO⁺ computed using the time-dependent wavepacket method with different PECs. Generally, all TD spectra essentially agree well with the experiment,[22] albeit with a noticeable method dependence.

For the two multiconfigurational methods employed, RASPT2 tends to underestimate the 0-1 peak intensity while RASSCF overestimates it. Moreover, over a wider energy range, the RASPT2 (RASSCF) spectrum exhibits a much faster (slower) decay in intensity with the increasing vibrational quantum number n , as compared to the experimental trend. In other words, the experiment spectrum is in between the RASSCF and RASPT2 predictions. Both methods adequately account for static correlation effects. However, RASSCF only treats dynamic correlation within the active space, whereas RASPT2 includes more dynamic correlation effects by perturbatively treating the effects of inactive orbitals. These results indicate the sensitivity of our calculations to the dynamic correlation.

In the case of DFT methods, there is substantially less variability among different functionals, indicating weak functional dependence. For a given functional, TD and TI spectra largely overlap, although some differences are observable. This is particularly evident with the BP86 functional, where TD spectra align excellently with the experiment while TI spectra noticeably underestimate the 0-1 peak intensity. The observed discrepancies can be partly attributed to differences in their complex numerical procedures and possibly the influence of anharmonic effects.

Figure 9(b) manifests similar performance at the O1s edge. In contrast to the behavior at the C1s edge, RASPT2 (RASSCF) overestimates (underestimates) the 0-1 peak and exhibits slower (faster) decay with n , demonstrating again the sensitive dependence on the treatment of dynamic correlation. At the DFT level, generally, TD models predict a slower decay with n compared to their corresponding TI method. Which one better agrees with the experiment depends on the functional. For instance, with the BP86 functional, the TD calculation accurately reproduces the experimental results, surpassing the TI method. Conversely, with the M06-2X functional, the TI calculation generates a better fit than its TD counterpart.

4.2.4 O1s XAS of NO⁺ and CO

As shown in Fig. 10(a-b), the O1s XAS spectra of NO⁺ and CO exhibit more complex vibronic structures than those observed for CO⁺, attributed to their larger geometrical changes induced by the O1s core hole. A noticeable discrepancy between the TD and TI methods is seen for each functional, with TD spectra predicting larger intensities mainly at the higher energy peaks (and sometimes also at the lower energy peaks). The inclusion of anharmonic effects in the TD calculations primarily accounts for this difference, thereby improving upon the TI approach.

A detailed comparison between the TD results and experimental data is offered in Fig. 11. Multiconfigurational methods (RASPT2 or MRPT3) give the best agreement to the experiments. In these spectra, each peak is identified by the vibrational quantum number n of the final state, and the one that labels the peak with the maximum intensity is denoted as n_{\max} . Remarkably, the multiconfigurational methods predict the same n_{\max} values ($n_{\max}=5$ for NO^+ ; $n_{\max}=4$ for CO) as those observed experimentally, while DFT predicts smaller n_{\max} values (mostly by 1). Our results indicate strong sensitivity of n_{\max} on the quality of the PECs.

Beyond the n_{\max} prediction, pure functionals BLYP and BP86 yield generally good agreement with experimental results in terms of both peak separations and intensities, despite their easy implementations. In the CO spectra, BLYP/BP86 exhibits a decay speed relative to n that aligns with experimental data, whereas MRPT3 predicts a slower rate of decay. These calculations underscore the solid performance of pure functionals, offering competitive accuracy compared to the more advanced and computationally-intensive multiconfigurational methods, and acceptable performance for hybrid functionals.

5 Summary and Conclusions

To summarize, we have conducted a comprehensive theoretical investigation of vibrationally-resolved X-ray spectra for diatomic systems using both the time-independent (TI) method with the harmonic oscillator approximation and the time-dependent (TD) wavepacket method. Within the TI framework, we systematically evaluated the vibrationally-resolved XAS (N_2 , N_2^+ , NO^+ , CO , and CO^+) and XPS (CO) spectra of several diatomic systems via DFT employing four different functionals. In most instances, the theoretical spectra exhibit good agreement with experimental results: pure functionals (BLYP and BP86) exhibited better or similar spectral accuracy to hybrid functionals (B3LYP and M06-2X), attributed to superior prediction accuracy in bond lengths and vibrational frequencies. Generally, functional dependence tends to be more sensitive in polyatomic systems, while its degree of sensitivity still depends on the system: pronounced dependence was observed in XAS spectra of N_2 , N_2^+ , and NO^+ , whereas slight dependence manifested in other cases. Two difficult cases were found for the O1s XAS of NO^+ and CO with numerous weak oscillating features, where the TI predictions underestimated the intensities for peaks with larger vibrational quantum numbers n . This discrepancy is mainly attributed to the anharmonic effects. Our analysis has related the two cases to their large geometrical changes as induced by the introduced core hole.

On the other hand, we also computed the XAS spectra of three systems (CO^+ , NO^+ , and CO) using the TD approach, based on potential energy curves (PECs) generated at both the DFT and multiconfigurational levels. For XAS spectra of CO^+ , all methods show good agreement while sensitivity to the dynamic correlation (multiconfigurational methods) and functional choice (DFT methods) is also visible. For challenging cases of the O1s XAS spec-

tra of NO^+ and CO, TD spectra significantly improved upon the corresponding TI results due to the superior consideration of anharmonic effects within the PECs. Thus, these findings underscore the centrality of anharmonicity to such problems, as previously evidenced in vibrationally-resolved X-ray [64] and ultraviolet-visible (UV) absorption spectra,[66] as well as vibrational (infrared and Raman) spectra.[67, 68] The pure functionals yielded results comparable in accuracy to the multiconfigurational methods and exhibited excellent agreement with experimental data. Our study illuminates the efficacy of DFT with pure functionals in predicting accurate vibrationally-resolved X-ray spectra, wherein the TI framework is optimal for most scenarios, but the TD framework should be employed for problems characterized by strong anharmonic effects.

The TI and TD approaches are complementary. TI can offer explicit spectral interpretations and direct insights into structural changes. Although in this study of diatomic systems, equilibrium bond length can be obtained from Morse fitting in TD calculations, this task becomes difficult for polyatomic systems. Conversely, TD proves superior when addressing complex diatomic cases involving anharmonic effects. Practical applications hinge on the ease and accuracy of excited-state geometry optimization or PEC scanning, and the significance of anharmonicity.

Acknowledgments

Part of this work was inspired by a previous collaborative study on NO^+ , and we thank Dr. Rebecka Lindblad for sending us the raw experimental XAS spectra of NO^+ and Prof. Hans Ågren and Dr. Rafael Couto for helpful discussions. We also appreciate valuable discussions with Prof. Chen Jing. Financial support from the National Natural Science Foundation of China (Grant No. 12274229) and the Postgraduate Research & Practice Innovation Program of Jiangsu Province (Grant Nos. KYCX22_0425 and KYCX22_0424) is greatly acknowledged.

References

- [1] Carravetta V, Couto R C and Ågren H 2022 *J. Phys.: Condens. Matter* **34** 363002
- [2] Hergenhahn U 2004 *J. Phys. B: At. Mol. Opt. Phys.* **37** R89–R135 and Fig. 5 therein, with the experimental C1s and O1s XPS spectra of CO, has been recaptured in our Fig. 6.
- [3] Svensson S 2005 *J. Phys. B: At. Mol. Opt. Phys.* **38** S821–S838
- [4] Siegbahn K 1969 *ESCA applied to free molecules* (North-Holland Publishing)

- [5] Gel’Mukhanov F, Mazalov L and Kondratenko A 1977 *Chem. Phys. Lett.* **46** 133–137
- [6] Chen C T, Ma Y and Sette F 1989 *Phys. Rev. A* **40** 6737–6740 ISSN 0556-2791 and Fig. 2(a) therein, with the experimental N1s XAS spectrum of N₂, has been recaptured in our Fig. 2(a).
- [7] Rennie E, Kempgens B, Köppe H, Hergenhahn U, Feldhaus J, Itchkawitz B, Kilcoyne A, Kivimäki A, Maier K, Piancastelli M and others 2000 *J. Chem. Phys.* **113** 7362–7375
- [8] Minkov I, Gel’Mukhanov F, Friedlein R, Osikowicz W, Suess C, Öhrwall G, Sorensen S L, Braun S, Murdey R, Salaneck W R and Ågren H 2004 *J. Chem. Phys.* **121** 5733–5739
- [9] Hoshino M, Montuoro R, Lucchese R R, De Fanis A, Hergenhahn U, Prümper G, Tanaka T, Tanaka H and Ueda K 2008 *J. Phys. B: At. Mol. Opt. Phys.* **41** 085105 ISSN 0953-4075, 1361-6455 URL <https://iopscience.iop.org/article/10.1088/0953-4075/41/8/085105>
- [10] Fronzoni G, Baseggio O, Stener M, Hua W, Tian G, Luo Y, Apicella B, Alfé M, de Simone M, Kivimäki A and Coreno M 2014 *J. Chem. Phys.* **141** 044313
- [11] Mosnier J P, Kennedy E T, van Kampen P, Cubaynes D, Guilbaud S, Sisourat N, Puglisi A, Carniato S and Bizau J M 2016 *Phys. Rev. A* **93** 061401(R)
- [12] Vaz da Cruz V, Ertan E, Ignatova N, Couto R C, Polyutov S, Odelius M, Kimberg V and Gel’Mukhanov F 2018 *Phys. Rev. A* **98** 012507
- [13] Michelitsch G S and Reuter K 2019 *J. Chem. Phys.* **150** 074104
- [14] Kjellsson L 2021 *X-ray spectroscopy on diatomic and cationic molecules* Ph.D. thesis Uppsala University
- [15] Huang M, Li C and Evangelista F A 2022 *J. Chem. Theory Comput.* **18** 219–233 ISSN 1549-9618, 1549-9626 and Fig. 3 therein, with the theoretical PECs of CO by MRPT3, has been recaptured in our Fig. 8(b).
- [16] Schippers S, Hillenbrand P, Perry-Sassmannshausen A, Buhr T, Fuchs S, Reinwardt S, Trinter F, Müller A and Martins M 2023 *ChemPhysChem* **24** e202300061 ISSN 1439-4235, 1439-7641
- [17] Cerezo J and Santoro F 2023 *J. Comput. Chem.* **44** 626–643 ISSN 0192-8651, 1096-987X
- [18] Duschinsky F 1937 *Acta Physicochim. URSS* **7**
- [19] Wei M, Cheng X, Zhang L, Zhang J R, Wang S Y, Ge G, Tian G and Hua W 2022 *Phys. Rev. A* **106** 022811 ISSN 2469-9926, 2469-9934

- [20] Wei M, Zhang L, Tian G and Hua W 2023 Vibronic fine structure in the nitrogen 1s photoelectron spectra from Franck-Condon simulations II: Indoles arXiv:2307.01510 [physics]
- [21] Gel'mukhanov F and Ågren H 1999 *Phys. Rep.* **312** 87–330 ISSN 03701573
- [22] Couto R C, Kjellsson L, Ågren H, Carravetta V, Sorensen S L, Kubin M, Bülow C, Timm M, Zamudio-Bayer V, von Issendorff B, Lau J T, Söderström J, Rubensson J E and Lindblad R 2020 *Phys. Chem. Chem. Phys.* **22** 16215–16223 and Fig. 2(a) therein, with the experimental C1s and O1s XAS spectra of CO⁺, has been recaptured in our Figs. 5 and 9, and Fig. 2(b) therein, with the RASPT2 PECs of CO⁺, has been recaptured in our Fig. 7.
- [23] Besley N A 2020 *Acc. Chem. Res.* **53** 1306–1315 ISSN 0001-4842, 1520-4898
- [24] Hua W, Tian G and Luo Y 2020 *Phys. Chem. Chem. Phys.* **22** 20014–20026 ISSN 1463-9076, 1463-9084
- [25] Cheng X, Wei M, Tian G, Luo Y and Hua W 2022 *J. Phys. Chem. A* **126** 5582–5593 ISSN 1089-5639, 1520-5215
- [26] Couto R C, Hua W, Lindblad R, Kjellsson L, Sorensen S L, Kubin M, Bülow C, Timm M, Zamudio-Bayer V, Von Issendorff B, Söderström J, Lau J T, Rubensson J E, Ågren H and Carravetta V 2021 *Phys. Chem. Chem. Phys.* **23** 17166–17176 ISSN 1463-9076, 1463-9084
- [27] Prendergast D and Galli G 2006 *Phys. Rev. Lett.* **96** 215502 ISSN 0031-9007, 1079-7114
- [28] Minkov I, Gelmukhanov F, Ågren H, Friedlein R, Suess C and Salaneck W R 2005 *J. Phys. Chem. A* **109** 1330–1336
- [29] Triguero L, Pettersson L G M and Ågren H 1998 *Phys. Rev. B* **58** 8097–8110
- [30] Jolly W L and Hendrickson D N 1970 *J. Am. Chem. Soc.* **92** 1863–1871
- [31] Ehara M, Nakatsuji H, Matsumoto M, Hatamoto T, Liu X J, Lischke T, Prümper G, Tanaka T, Makochekanwa C, Hoshino M, Tanaka H, Harries J R, Tamenori Y and Ueda K 2006 *J. Chem. Phys.* **124** 124311 ISSN 0021-9606, 1089-7690
- [32] Püttner R, Dominguez I, Morgan T J, Cisneros C, Fink R F, Rotenberg E, Warwick T, Domke M, Kaindl G and Schlachter A S 1999 *Phys. Rev. A* **59** 3415–3423 ISSN 1050-2947, 1094-1622 and Fig. 1 therein, with the experimental O1s XAS spectrum of CO, has been recaptured in our Fig. 4(b), Fig. 10(b), and Fig. 11(b)
- [33] Carniato S, Bizau J M, Cubaynes D, Kennedy E T, Guilbaud S, Sokell E, McLaughlin B and Mosnier J P 2020 *Atoms* **8** 67 ISSN 2218-2004

- [34] Lindblad R, Kjellsson L, Couto R C, Timm M, Bülow C, Zamudio-Bayer V, Lundberg M, von Issendorff B, Lau J T, Sorensen S L, Carravetta V, Ågren H and Rubensson J E 2020 *Phys. Rev. Lett.* **124** 203001 ISSN 0031-9007, 1079-7114 and Fig. 2 therein, with the experimental N1s XAS spectra of N_2^+ , has been recaptured in our Fig. 2(b).
- [35] Lindblad R, Kjellsson L, De Santis E, Zamudio-Bayer V, von Issendorff B, Sorensen S L, Lau J T, Hua W, Carravetta V, Rubensson J E, Ågren H and Couto R C 2022 *Phys. Rev. A* **106** 042814 ISSN 2469-9926, 2469-9934 and Fig. 3 therein, with the XAS spectra of NO^+ (experimental, N1s/O1s; RASPT2, O1s), has been recaptured in our Figs. 3, 10(a), and 11(a).
- [36] Rocha A B 2011 *J. Chem. Phys.* **134** 024107
- [37] Martins M, Reinwardt S, Schunck J O, Schwarz J, Baev K, Müller A, Buhr T, Perry-Sassmannshausen A, Klumpp S and Schippers S 2021 *J. Phys. Chem. Lett.* **12** 1390–1395
- [38] Sharp T and Rosenstock H 1964 *J. Chem. Phys.* **41** 3453–3463
- [39] Ruhoff P T 1994 *Chem. Phys.* **186** 355–374
- [40] Ruhoff P T and Ratner M A 2000 *Int. J. Quantum Chem.* **77** 383–392
- [41] Bagus P S 1965 *Phys. Rev.* **139**(3A) A619–A634
- [42] Triguero L, Plashkevych O, Pettersson L and Ågren H 1999 *J. Electron. Spectrosc. Relat. Phenom.* **104** 195–207 ISSN 03682048
- [43] Gordon M S and Schmidt M W 2005 Advances in electronic structure theory *Theory and Applications of Computational Chemistry* (Elsevier) pp 1167–1189 ISBN 978-0-444-51719-7
- [44] Schmidt M W, Baldrige K K, Boatz J A, Elbert S T, Gordon M S, Jensen J H, Koseki S, Matsunaga N, Nguyen K A, Su S, Windus T L, Dupuis M and Montgomery J A 1993 *J. Comput. Chem.* **14** 1347–1363 ISSN 0192-8651, 1096-987X
- [45] Becke A D 1988 *Phys. Rev. A* **38** 3098–3100 ISSN 0556-2791
- [46] Lee C, Yang W and Parr R G 1988 *Phys. Rev. B* **37** 785–789 ISSN 0163-1829
- [47] Perdew J P 1986 *Phys. Rev. B* **33** 8822–8824 ISSN 0163-1829
- [48] Becke A D 1993 *J. Chem. Phys.* **98** 5648–5652 ISSN 0021-9606, 1089-7690
- [49] Zhao Y and Truhlar D G 2008 *Theor. Chem. Acc.* **119** 525–525 ISSN 1432-881X, 1432-2234
- [50] Dunning T H 1989 *J. Chem. Phys.* **90** 1007–1023 ISSN 0021-9606, 1089-7690

- [51] Kendall R A, Dunning T H and Harrison R J 1992 *J. Chem. Phys.* **96** 6796–6806 ISSN 0021-9606, 1089-7690
- [52] Kutzelnigg W, Fleischer U and Schindler M 1990 The IGLO-Method: Ab-initio Calculation and Interpretation of NMR Chemical Shifts and Magnetic Susceptibilities *Deuterium and Shift Calculation* vol 23 ed Diehl P, Fluck E, Günther H, Kosfeld R and Seelig J (Berlin, Heidelberg: Springer Berlin Heidelberg) pp 165–262 ISBN 978-3-642-75934-5 978-3-642-75932-1 series Title: NMR Basic Principles and Progress
- [53] Sakai Y, Miyoshi E, Klobukowski M and Huzinaga S 1997 *J. Chem. Phys.* **106** 8084–8092
- [54] Noro T, Sekiya M and Koga T 1997 *Theor. Chem. Acc.* **98** 25–32
- [55] Segmented Gaussian Basis Set. <http://sapporo.center.ims.ac.jp/sapporo/>. Accessed on 2023-7-4.
- [56] See Supplemental Material at [URL will be inserted by publisher] for optimized Cartesian coordinates of all systems and PEC data as used in Figs. 7–8.
- [57] Zschornack G H 2007 *Handbook of X-Ray Data* (New York: Springer)
- [58] Werner H J, Knowles P J, Knizia G, Manby F R and Schütz M 2012 *WIREs Comput Mol Sci* **2** 242–253
- [59] Hua W, Mukamel S and Luo Y 2019 *J. Phys. Chem. Lett.* **10** 7172–7178 ISSN 1948-7185, 1948-7185
- [60] Hua W, Bennett K, Zhang Y, Luo Y and Mukamel S 2016 *Chem. Sci.* **7** 5922–5933 ISSN 2041-6520, 2041-6539
- [61] Zhang Y, Hua W, Bennett K and Mukamel S 2016 *Top. Curr. Chem.* **368** 273–345
- [62] Hua W and Wei M XSpecTime, version 0.9 Nanjing University of Science and Technology: Nanjing, 2023
- [63] Neeb M, Rubensson J E, Biermann M and Eberhardt W 1994 *J. Electron. Spectrosc. Relat. Phenom.* **67** 261–274 ISSN 03682048
- [64] Moitra T, Madsen D, Christiansen O and Coriani S 2020 *J. Chem. Phys.* **153** 234111 ISSN 0021-9606, 1089-7690
- [65] Hitchcock A and Brion C 1980 *J. Electron. Spectrosc. Relat. Phenom.* **18** 1–21 ISSN 03682048 and Figs. 5 and 6(a) therein, with the experimental N1s XAS spectrum of N₂ and C1s XAS spectrum of CO, have been recaptured in our Fig. 2(a) and 4(a), respectively.

- [66] Madsen D, Christiansen O, Norman P and König C 2019 *Phys. Chem. Chem. Phys.* **21** 17410–17422 ISSN 1463-9076, 1463-9084
- [67] Brauer B, Gerber R B, Kabeláč M, Hobza P, Bakker J M, Abo Riziq A G and De Vries M S 2005 *J. Phys. Chem. A* **109** 6974–6984 ISSN 1089-5639, 1520-5215
- [68] Panek P T and Jacob C R 2016 *J. Phys. Chem. Lett.* **7** 3084–3090 ISSN 1948-7185, 1948-7185
- [69] Albritton D L, Schmeltekopf A L and Zare R N 1979 *J. Chem. Phys.* **71** 3271–3279 ISSN 0021-9606, 1089-7690
- [70] Laher R R and Gilmore F R 1991 *J. Phys. Chem. Ref. Data* **20** 685–712 ISSN 0047-2689, 1529-7845
- [71] Morse P M 1929 *Phys. Rev.* **34** 57–64 ISSN 0031-899X

TABLE I. Comparison of bond lengths (in Å) in the optimized ground (R') and 1s excited/ionized (R) states of all diatomic systems predicted by DFT with different functionals.

Compound	Expt.			BLYP			BP86			B3LYP			M06-2X		
	R'	R	ΔR^a	R'	R	ΔR	R'	R	ΔR	R'	R	ΔR	R'	R	ΔR
N ₂	1.098 ^{e, †}	1.164 ^{f, i}	+0.066	1.103	1.167	+0.063	1.103	1.164	+0.061	1.092	1.137	+0.046	1.087	1.130	+0.044
N ₂ ⁺	1.116 ^f	1.076	-0.040 ^j	1.116	1.078	-0.038	1.115	1.078	-0.038	1.105	1.051	-0.054	1.099	1.039	-0.061
NO ⁺ (N) ^b	1.063 ^g	1.123	+0.060 ^k	1.072	1.129	+0.058	1.071	1.125	+0.055	1.057	1.117	+0.059	1.050	1.109	+0.059
NO ⁺ (O)	1.063	1.203	+0.140 ^k	1.072	1.211	+0.139	1.071	1.205	+0.134	1.057	1.199	+0.141	1.050	1.193	+0.142
CO(C)	1.128 ^{f, h}	1.153 ^f	+0.025	1.138	1.164	+0.026	1.138	1.161	+0.023	1.126	1.156	+0.029	1.122	1.155	+0.034
CO(O)	1.128	1.291 ^h	+0.163	1.138	1.300	+0.162	1.138	1.295	+0.157	1.126	1.292	+0.165	1.122	1.293	+0.172
CO ⁺ (C)	1.115 ^f	1.078	-0.037 ^l	1.125	1.080	-0.045	1.124	1.080	-0.044	1.110	1.068	-0.043	1.102	1.059	-0.044
CO ⁺ (O)	1.115	1.162	+0.047 ^l	1.125	1.176	+0.051	1.124	1.175	+0.051	1.110	1.163	+0.052	1.102	1.156	+0.054
CO(C)[XPS] ^c	1.128	1.063	-0.065 ^m	1.138	1.080	-0.058	1.138	1.080	-0.059	1.126	1.068	-0.059	1.122	1.059	-0.063
CO(O)[XPS]	1.128	1.165	+0.037 ^m	1.138	1.176	+0.038	1.138	1.175	+0.037	1.126	1.163	+0.036	1.122	1.156	+0.035
MAD ^d	-	-	-	0.008	0.008	0.003	0.008	0.006	0.004	0.005	0.008	0.006	0.010	0.014	0.008
MAX ^d	-	-	-	0.010	0.017	0.008	0.010	0.017	0.007	0.011	0.027	0.020	0.017	0.037	0.022

^a $\Delta R \equiv R - R'$, changes of bond length in Å.

^b Core excitation/ionization center specified in parenthesis.

^c [XPS] denotes the comparison of initial and final states involved in XPS. The rest are for XAS.

^d MAD, mean absolute derivation; MAX, maximum absolute deviation.

^e Ehara et al.[31]

^f Neeb et al.[63]

^g Albritton et al.[69]

^h Püttner et al.[32]

ⁱ Chen et al.[6]

^j Lindblad et al.[34]

^k Lindblad et al.[35]

^l Couto et al.[22]

^m Hergenahn.[2]

Table 2:

TABLE II. Comparison of vibrational frequencies (in cm^{-1}) in the optimized ground (ω') and 1s excited/ionized (ω) states of all diatomic systems predicted by DFT with different functionals.

Compound	Expt.			BLYP			BP86			B3LYP			M06-2X		
	ω'	ω	$\Delta\omega^a$	ω'	ω	$\Delta\omega$	ω'	ω	$\Delta\omega$	ω'	ω	$\Delta\omega$	ω'	ω	$\Delta\omega$
N ₂	2359.0 ^e	1966.2 ^f	-392.8	2334.9	1938.0	-396.9	2345.7	1963.5	-382.2	2449.1	2175.3	-273.8	2522.6	2255.9	-266.7
N ₂ ⁺	2207.4 ^f	2420.8 ^g	+213.4	2234.1	2442.3	+208.1	2253.3	2456.8	+203.5	2330.2	2735.8	+405.6	2407.2	2896.2	+489.1
NO ⁺ (N) ^b	2376.7 ^h	1954.3 ⁱ	-422.4	2333.3	1987.8	-345.6	2353.6	2027.3	-326.2	2479.1	2077.5	-401.6	2587.6	2226.7	-360.9
NO ⁺ (O)	2376.7	1534.9 ^j	-841.8	2333.3	1512.6	-820.8	2353.6	1553.1	-800.5	2479.1	1584.1	-895.0	2587.6	1647.4	-940.2
CO(C)	2169.8 ^f	2083.6 ^f	-86.2	2114.5	2015.8	-98.8	2121.0	2042.6	-78.4	2210.9	2091.3	-119.7	2273.9	2130.4	-143.5
CO(O)	2169.8	1338.9 ⁱ	-830.9	2114.5	1264.8	-849.7	2121.0	1292.1	-828.9	2210.9	1302.0	-908.9	2273.9	1304.0	-969.9
CO ⁺ (C)	2214.2 ^f	2507.6 ^k	+293.4	2172.5	2478.6	+306.1	2192.0 ^m	2490.0	+298.0	2289.8	2612.5	+322.7	2393.3	2748.2	+354.9
CO ⁺ (O)	2214.2	1817.2 ^k	-397.0	2172.5	1779.0	-393.5	2192.0	1787.9	-404.1	2289.8	1875.3	-414.6	2393.3	1939.3	-454.0
CO(C)[XPS] ^c	2169.8	2451.9 ^l	+282.1	2114.5	2478.6	+364.1	2121.0	2490.0	+368.9	2210.9	2612.5	+401.6	2273.9	2748.2	+474.4
CO(O)[XPS]	2169.8	1822.8 ^l	-347.0	2114.5	1779.0	-335.5	2121.0	1787.9	-333.1	2210.9	1875.3	-335.6	2273.9	1939.3	-334.5
MAD ^d	-	-	-	44.2	38.5	24.8	34.5	33.8	28.0	73.3	111.7	67.5	156.0	200.7	108.1
MAX ^d	-	-	-	55.3	74.1	82.0	48.8	73.0	96.2	122.8	315.0	192.2	210.9	475.4	275.7

^a $\Delta\omega \equiv \omega - \omega'$, changes of frequency in cm^{-1} .

^b Core excitation/ionization center specified in parenthesis.

^c [XPS] denotes the comparison of initial and final states involved in XPS. The rest are for XAS.

^d MAD, mean absolute derivation; MAX, maximum absolute deviation.

^e Ehara et al.[31]

^f Neeb et al.[63]

^g Laher et al.[70]

^h Albritton et al.[69]

ⁱ Püttner et al.[32]

^j Lindblad et al.[35]

^k Couto et al.[22]

^l Hergenbahn.[2]

^m By restricted open-shell DFT (RO-DFT; the rest are by unrestricted DFT).

Table 3: Fitted Morse[71] parameters for the potential energy curves of CO⁺, CO, and NO in the ground and the lowest 1s excited states by using different electronic structure methods. All parameters are in atomic units.

Method	T_e^a	D_e	α	R_e
CO⁺ ground				
RASPT2 ^b	0.0023	0.3528	1.3600	2.0947
RASSCF	0.0043	0.3206	1.4663	2.0839
BLYP	-0.0002	0.3524	1.3257	2.1210
BP86	-0.0003	0.3660	1.3131	2.1196
B3LYP	0.0015	0.3489	1.4016	2.0847
M06-2X	0.0027	0.3738	1.4132	2.0661
CO⁺ C1s				
RASPT2	10.3539	0.3133	1.5421	2.0330
RASSCF	10.4314	0.3643	1.6221	1.9895
BLYP	10.3655	0.3592	1.4681	2.0387
BP86	10.3541	0.3578	1.4820	2.0353
B3LYP	10.3679	0.3590	1.5336	2.0109
M06-2X	10.3665	0.4558	1.4540	1.9926
CO⁺ O1s				
RASPT2	19.4320	0.2778	1.3205	2.2142
RASSCF	19.5124	0.2855	1.4308	2.1339
BLYP	19.4007	0.2596	1.3102	2.2217
BP86	19.3969	0.2394	1.3607	2.2143
B3LYP	19.3918	0.2961	1.2893	2.1978
M06-2X	19.3765	0.3481	1.2336	2.1899
NO⁺ ground				
BLYP	-0.0021	0.4695	1.2793	2.0388
BP86	-0.0022	0.4884	1.2657	2.0372
B3LYP	-0.0015	0.5644	1.2339	2.0132
M06-2X	-0.0014	0.6730	1.1780	2.0004
NO⁺ O1s				
BLYP	19.5858	0.1591	1.4631	2.2769
BP86	19.5814	0.1693	1.4535	2.2663
B3LYP	19.6141	0.1782	1.4643	2.2442
M06-2X	19.6623	0.2132	1.4301	2.2176
CO ground				
MRPT3 ^c	0.0018	0.4239	1.2168	2.1346
BLYP	-0.0031	0.4149	1.2078	2.1560
BP86	-0.0032	0.4272	1.1961	2.1565
B3LYP	-0.0033	0.4791	1.1739	2.1360
M06-2X	-0.0035	0.5436	1.1345	2.1288
CO O1s				
MRPT3	19.6227	0.1751	1.1700	2.4475
BLYP	19.5558	0.1407	1.3100	2.4375
BP86	19.5508	0.1460	1.3092	2.4274
B3LYP	19.5784	0.1378	1.3528	2.4091
M06-2X	19.6100	0.1870	1.2649	2.3850

^a $U(R) = T_e + D_e[1 - e^{-\alpha(R-R_e)}]^2$. R_e , equilibrium internuclear distance; D_e , dissociation energy (well depth); $\alpha = \sqrt{k_c/2D_e}$, a potential width parameter; $k_c = [\frac{d^2U(R)}{dR^2}]_{R=R_e}$, force constant at R_e ; T_e , a constant term.

^b RASPT2 PECs are from Couto et al.[22]

^c MRPT3 PECs are from Huang et al.[15]

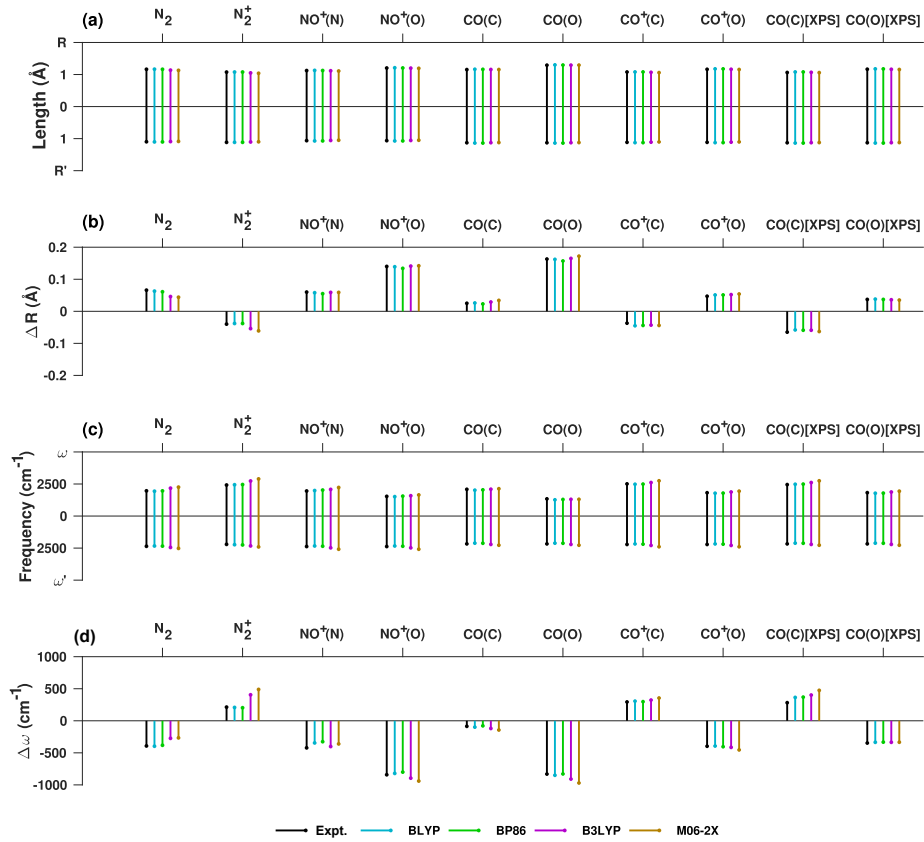


Figure 1: Parameters of diatomic systems at their DFT-optimized structures in both the ground and excited states with various functionals: (a) bond lengths in the ground (R') and excited (R) states, (b) changes in bond length (ΔR), (c) vibrational frequencies in the ground (ω') and excited (ω) states, and (d) changes in frequency ($\Delta\omega$). Here the excited state refers to the lowest C/N/O 1s ionized (labeled by XPS in brackets) or excited (the rest) state, with the excited atom denoted in parentheses where necessary. Corresponding theoretical and experimental data are listed in Tables 1 and 2.

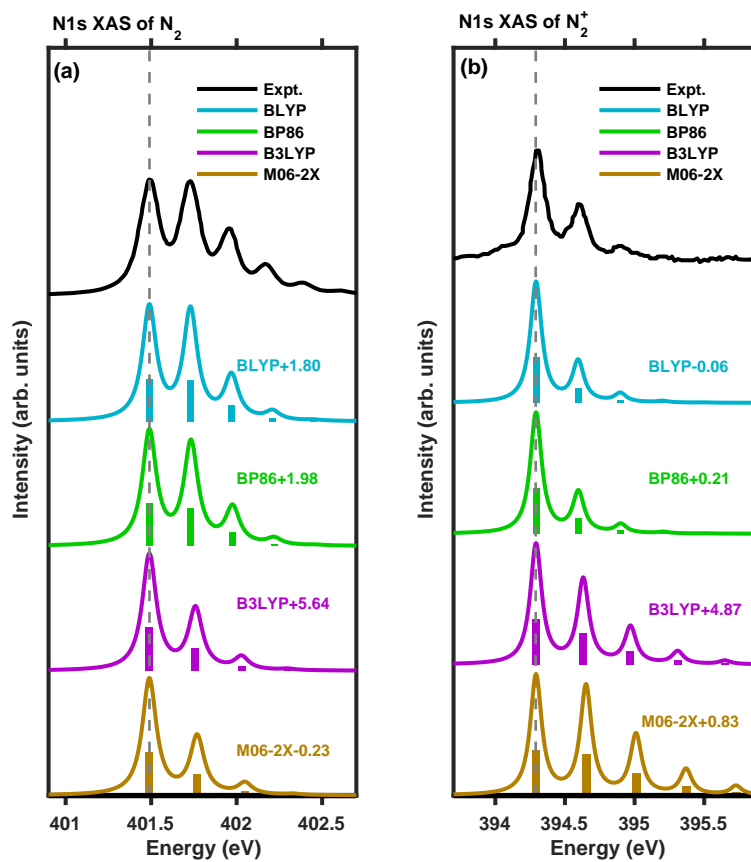


Figure 2: Vibrationally-resolved N1s XAS spectra of (a) N_2 and (b) N_2^+ simulated in the time-independent framework with different DFT functionals. To better compare with the experiments,[6, 65, 34] theoretical spectra have been shifted (indicated by numbers in eV) by aligning the first peak.

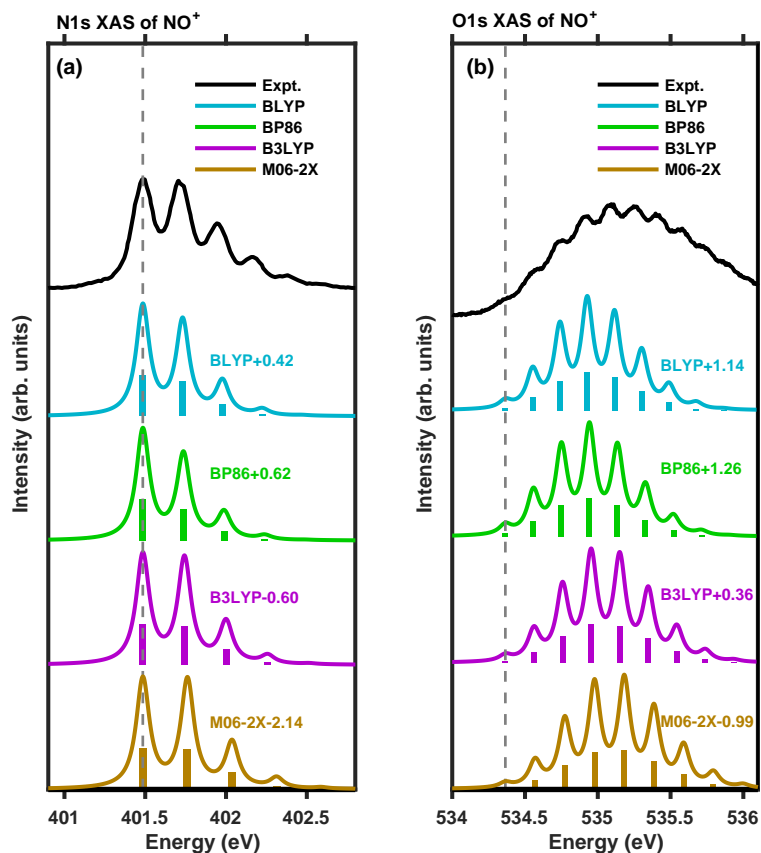


Figure 3: Vibrationally-resolved XAS spectra of NO^+ simulated in the time-independent framework with different DFT functionals: (a) N1s and (b) O1s edges. To better compare with the experiment,[35] theoretical spectra have been shifted (indicated by numbers in eV) by aligning the first peak.

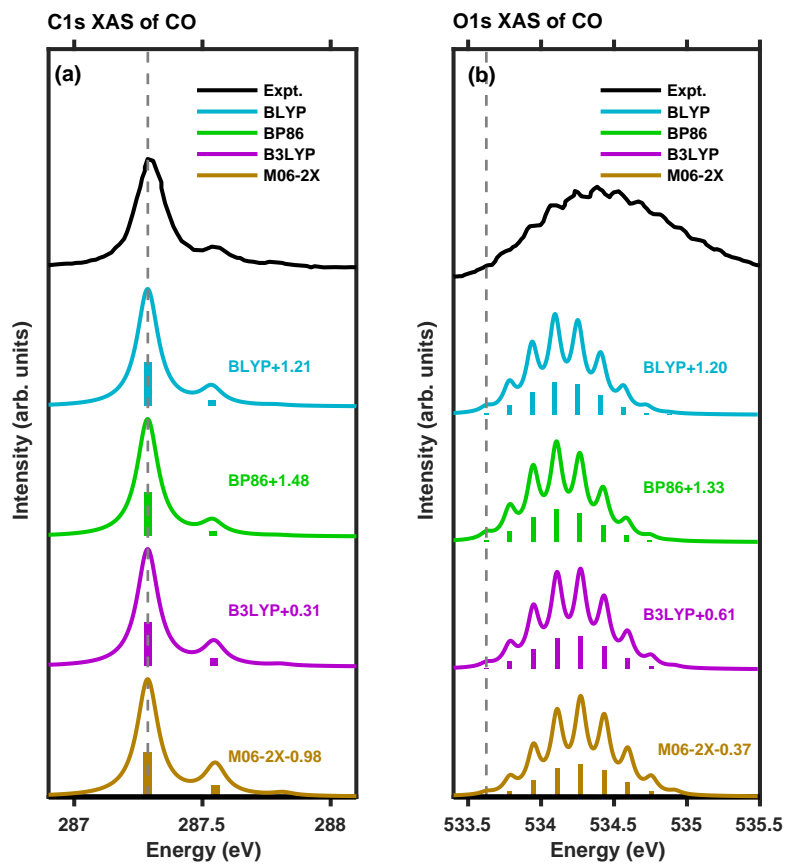


Figure 4: Vibrationally-resolved XAS spectra of CO simulated in the time-independent framework with different DFT functionals: (a) C1s and (b) O1s edges. To better compare with the experiments at the C1s[65] and O1s[32] edges, theoretical spectra have been shifted (indicated by numbers in eV) by aligning the first peak.

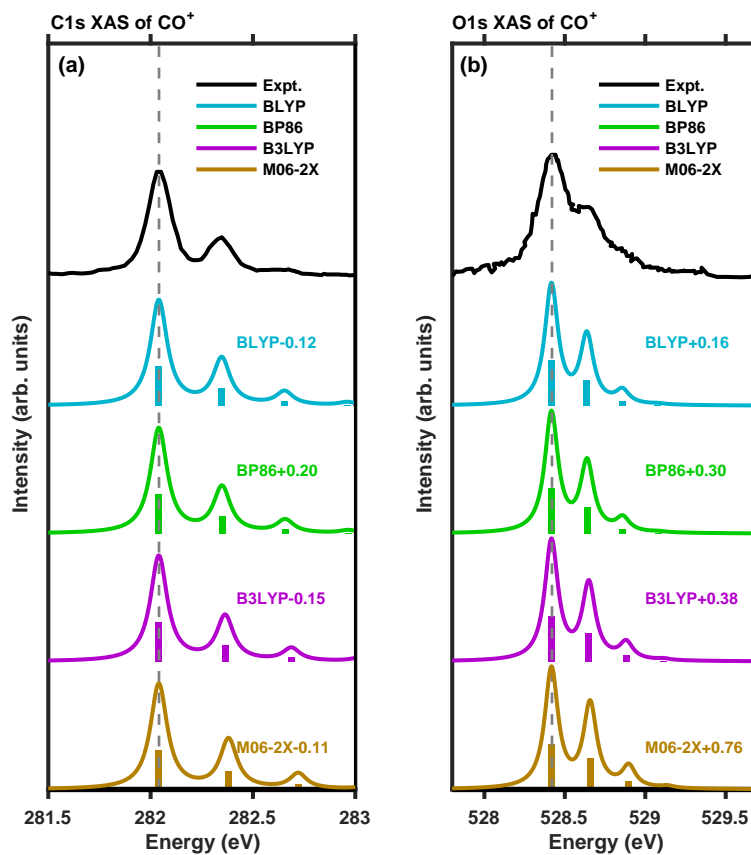


Figure 5: Vibrationally-resolved XAS spectra of CO^+ simulated in the time-independent framework with different DFT functionals: (a) C1s and (b) O1s edges. To better compare with the experiment,[22] theoretical spectra have been shifted (indicated by numbers in eV) by aligning the first peak.

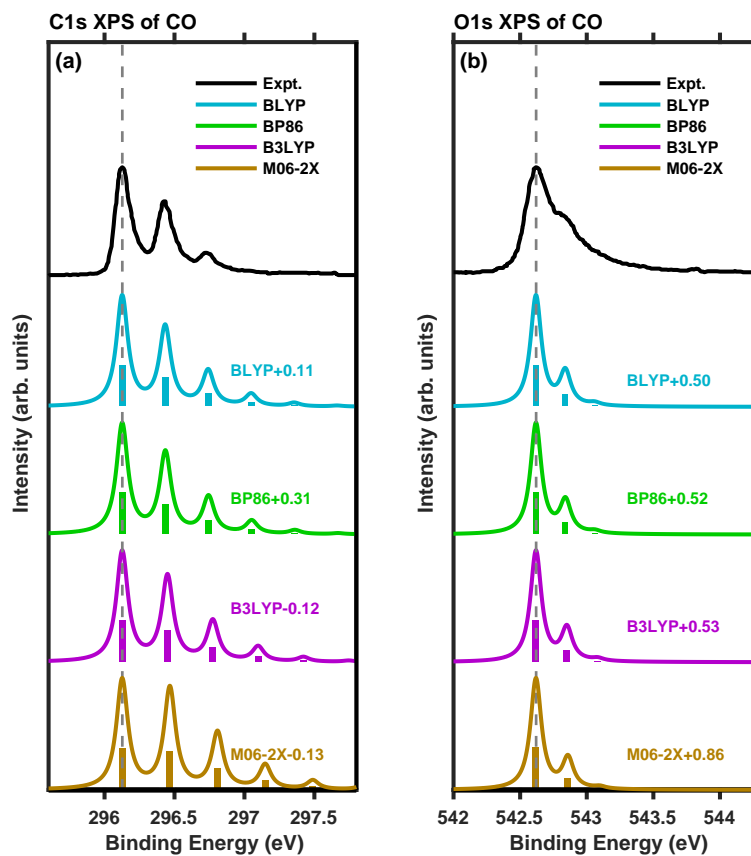


Figure 6: Vibrationally-resolved XPS spectra of CO simulated in the time-independent framework with different DFT functionals: (a) C1s and (b) O1s edges. To better compare with the experiment,[2] theoretical spectra have been shifted (indicated by numbers in eV) by aligning the first peak.

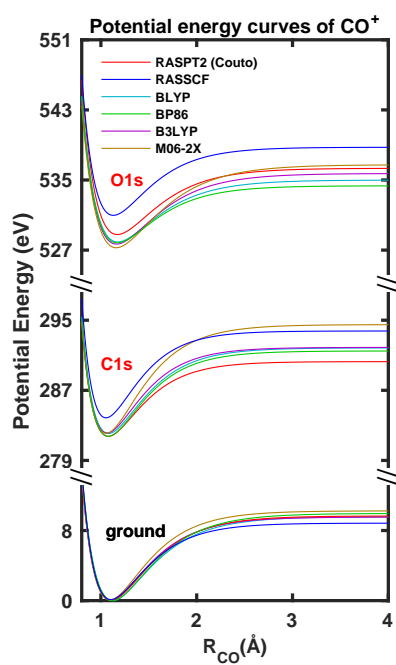


Figure 7: Simulated potential energy curves of CO⁺ in the ground, the lowest C and O 1s electron excited states by using different theoretical methods. RASPT2 curves were taken from Couto et al.[22]

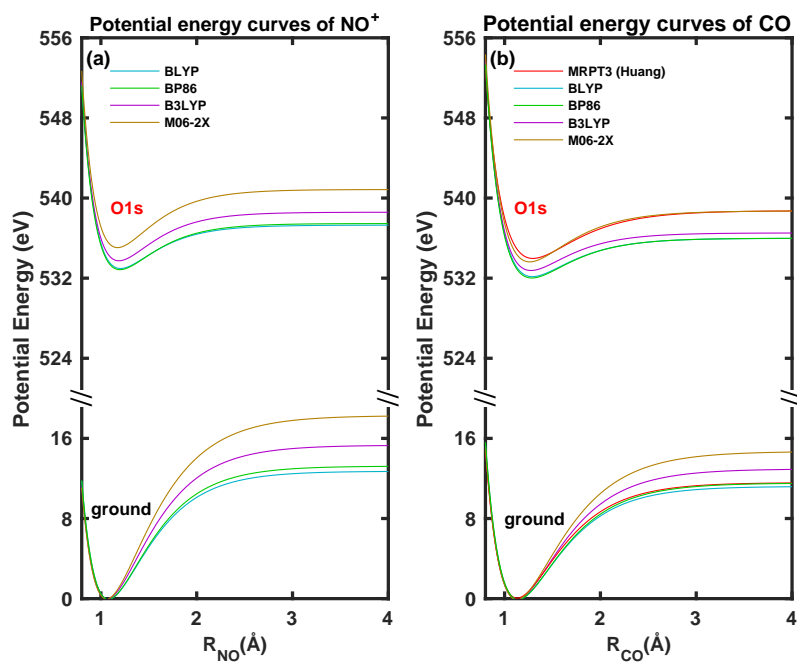


Figure 8: Simulated potential energy curves of (a) NO⁺ and (b) CO in the lowest O1s excited state by different theoretical methods. In the lower part of each panel, the ground state PECs simulated by the same method are also shown. In panel b, MRPT3 curves of CO were taken from Huang et al.[15]

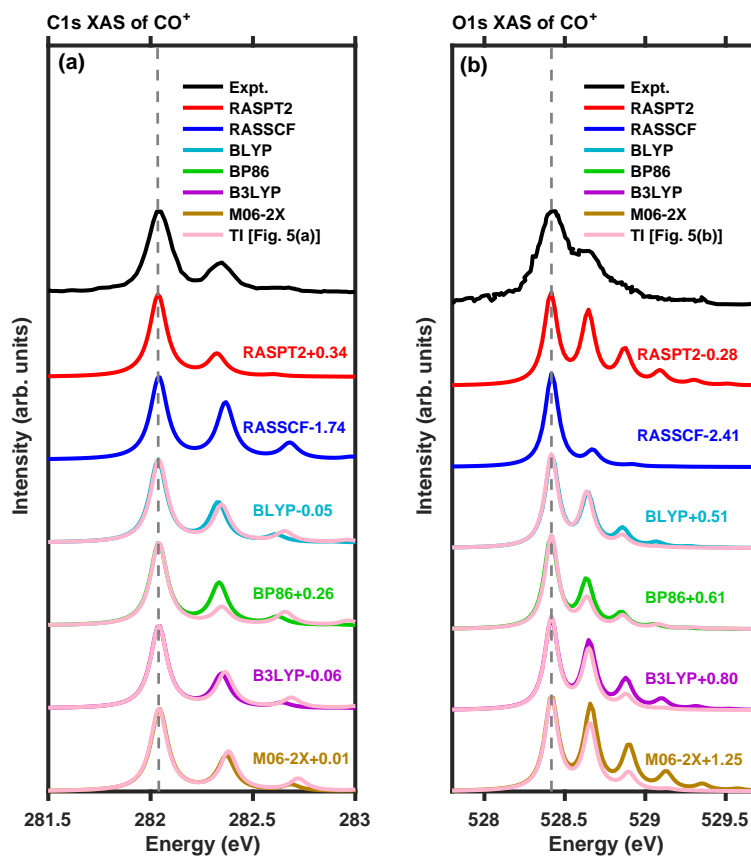


Figure 9: Comparison of vibrationally-resolved XAS of CO^+ simulated by the time-dependent (other colored lines) and time-independent (pink lines; recaptured from Fig. 5) methods: (a) C1s and (b) O1s edges. Different electronic structure methods are used, where “RASPT2” denotes our calculated spectra using RASPT2 PECs (see Fig. 7) from Couto et al.,[22] while the rest of theoretical lines are purely our results. To better compare with the experiments,[22] theoretical spectra have been shifted (indicated by numbers in eV) by aligning the first peak.

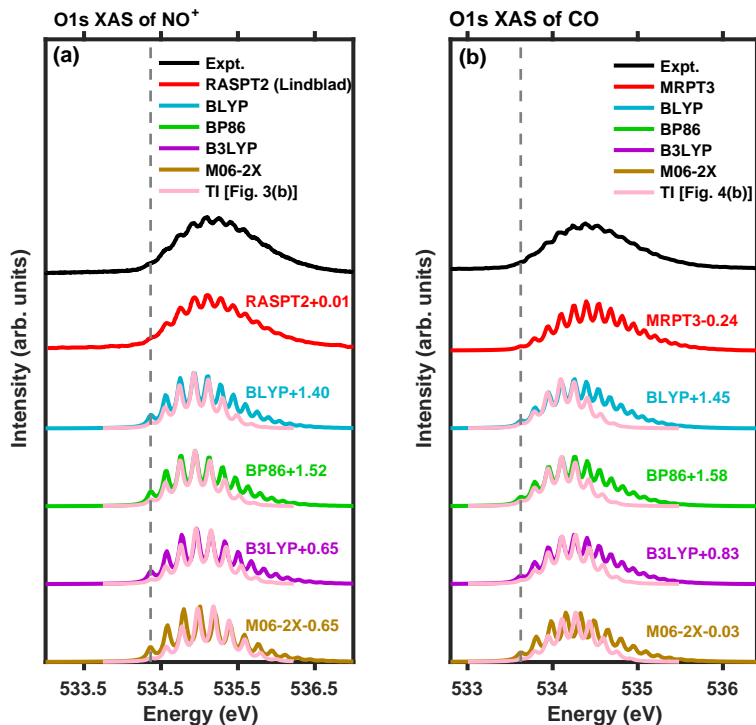


Figure 10: Comparison of vibrationally-resolved XAS spectra of (a) NO^+ and (b) CO simulated by the time-dependent (other colored lines) and time-independent [pink lines; recaptured from Figs. 3(b) and 4(b), respectively] methods. Different electronic structure methods are used. In panel a, the RASPT2 spectrum was taken from Lindblad et al.[35] In panel b, “MRPT3” denotes our calculated spectrum using MRPT3 PECs [see Fig. 8(b)] from Huang et al.[15] The rest of theoretical lines are purely our results. To better compare with the experiments of NO^+ [35] and CO ,[32] theoretical spectra have been shifted (indicated by numbers in eV) by aligning the first peak.

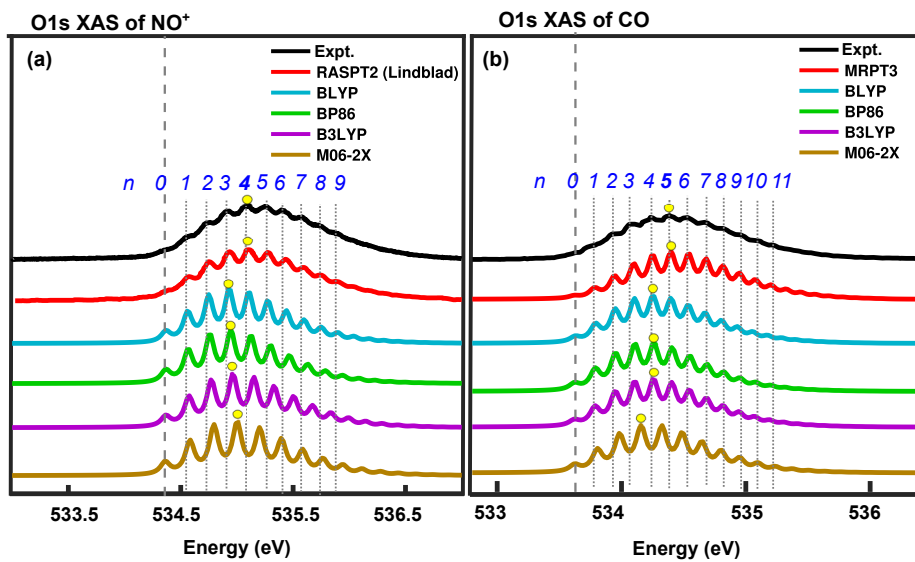


Figure 11: Close-up view of Fig. 10 with only the TD results and experiments. The experimental spectra are interpreted with the final-state quantum number n (dashed and dotted lines are to guide eyes). In each panel, the peak with the largest intensity (n_{\max}) is in bold font, and the circle labels n_{\max} as predicted by each method.